Environ Geol (2007) 52:215–224
DOI 10.1007/s00254-006-0475-y

ORIGINAL ARTICLE

The influence of petrophysical properties on the salt weathering of porous building rocks

D. Benavente · N. Cueto · J. Martínez-Martínez · M. A. García del Cura · J. C. Cañaveras

Received: 16 June 2006 / Accepted: 16 August 2006 / Published online: 13 September 2006

Abstract The influence of pore structure, water transport properties and rock strength on salt weathering is evaluated by means of a thorough rock characterisation and a statistical analysis. The pore structure was described in terms of its porosity, pore size distribution (quantified by mean pore radius) and specific surface area, density and water transport was characterised by means of water permeability (saturated flow) and capillary imbibition (unsaturated flow); whilst the rock strength test was carried out using uniaxial compressive strength, compressional and shear wave velocities, dynamic elastic constants and waveform energy and attenuation were obtained from the digital analysis of the transmitted signal. A principal component analysis and a stepwise multiple regression model was carried out in order to examine the direct relationships between salt weathering and petrophysical properties. From the principal component analysis, two main components were obtained and assigned a petrophysical meaning. The first component is mostly linked to mechanical properties, porosity and density whereas the second component is associated with the water transport and pore structure. Salt weathering, quantified by the percentage of weight loss after salt crystallisation, was included in both principal components, showing its dependence on their petrophysical properties. The stepwise multiple regression analysis found that rock strength has a predominant statistical weight in the prediction of salt weathering, with a minor contribution of water transport and pore structure parameters.

Keywords Building stone · Durability · Permeability · Petrophysics · Pore structure · Principal component analysis · Rock strength · Salt weathering

D. Benavente (✉) · N. Cueto · J. Martínez-Martínez · J. C. Cañaveras
Departamento de Ciencias de la Tierra y del Medio Ambiente, Universidad de Alicante, Ap. 99, Alicante 03080, Spain
e-mail: david.benavente@ua.es

M. A. García del Cura · D. Benavente · N. Cueto · J. Martínez-Martínez · J. C. Cañaveras
Laboratorio de Petrología Aplicada, Unidad Asociada CSIC-UA, Alicante, Spain

M. A. García del Cura
Instituto de Geología Económica, CSIC-UCM, Madrid, Spain

Introduction

Linking the durability of building rocks to their petrophysical properties, including water flow, pore structure and strength, has been a long-term aim which has generated great interest in many fields such as engineering geology, material science, architecture and earth sciences. Salt weathering of soluble salts is one of the most important decay processes that affect the durability of these rocks. A number of factors influence salt crystallisation damage in porous materials, including (1) pore size and porosity; (2) the nature of the salt, the ease with which it achieves high saturations by evaporation and/or variations in environmental temperature and, the energy difference between the crystal and the pore wall; (3) the transport of the solution, in terms of the supply rate of the solution and the evaporation of water and (4) strength, which is the material's resistance to crystallisation pressure.

In this paper, we apply a principal component analysis to examine direct relationships between salt weathering and water transport properties, pore structure and rock strength, which are particularly interesting parameters for interpreting damage processes. We particularly focus the study on two important factors: on the one hand, water transport in both saturated (permeability) and non-saturated (capillarity imbibition) conditions and their influence on durability in terms of pore structure; and, on the other, rock strength by means of the digital analysis of the transmitted ultrasonic waveform, which is compared with uniaxial compressive strength and linked to salt crystallisation damage.

Experimental procedures

Materials

In this study, 18 samples of porous stones have been chosen for their different petrophysical and petrographic characteristics. These stones are marketed and used as building materials and are highly homogeneous not only in the hand specimen but also in the quarry (Benavente 2003). The stones tested correspond to five types of sedimentary rocks which show different percentages of allochem (framework grains) and ortochem (e.g. cement) components and different sizes of allochem grains: quartz sandstone (QS), calcite sandstone (CS), calcite–quartz sandstone (CQS), dolomite sandstone (DS) and calcite–quartz conglomerate (CQC).

QS is a siliciclastic rock, more specifically, a quartz–arenite, while the other types are mechanically deposited limestones or dolostones in which the framework grains (allochems) are mainly bioclasts. CS and CQS types are calcarenite limestones consisting predominantly (>50%) of sand-size carbonate grains. CQC type is a calcirudite consisting predominantly of gravel-size carbonate (mainly fossils) grains. DS type is a dolarenite, a dolomite rock consisting predominantly of detrital sand-size dolomite grains. Next, a detailed description of the different rock types is shown:

Quartz sandstones (QS) are well-sorted arenites mainly composed of monocrystalline quartz grains (>95%). Feldspars, metamorphic rock fragments, chert and muscovite grains are accessory constituents. This sandstone is well cemented by secondary (authigenic) quartz in the form of overgrowth on the detrital grains. The formation of cement decreases the primary interparticle porosity

In calcite sanstones (CS) the framework grains are mainly foraminifers and less frequently of quartz, feldspar, rock fragments and micas (less than 3%). Foraminifers (mainly *Globigerinae*) are usually 0.1–0.2 mm in size. The orthochem component is micrite (≈2 μm). The main porosity types are intraparticle and vuggy.

Calcite–quartz sandstones (CQS) are well-sorted sandstones with calcite grains as the main framework constituent. Allochem calcite grains consist of 0.2–0.5 mm-thick foraminifers (mainly *Globigerinae*). Quartz, feldspars, micas, dolostones and other lithic grains are also present. Of these quartz is the most abundant. The ortochem component is calcite cement as equant mesocrystalline mosaics. The relative proportions of interparticle and intraparticle porosity are different in each sample.

Dolomite sandstone (DS) is a well-sorted sandstone consisting of dolomite (approximately 73% of the rock volume) and calcite (approximately 22% of the rock volume) grains. Detrital quartz grains (3–5%) and clay minerals (<2%) are minor constituents of the sandstone. The ortochem is mesocrystalline calcite cement. Interparticle porosity is very abundant.

Calcite–quartz conglomerates (CQC) are unsorted medium- to coarse-grained (0.02–10 mm) clastic rock. The framework mineralogy mainly consists of allochem calcite grains (bryozoans, red algae, mollucs and echinoderms). Other detrital components are quartz, limeclasts and feldspars. The ortochems (cements) are scarce, mainly consist of microcrystalline drusy calcite mosaics. Interpaticle porosity is very abundant whereas the proportion of intraparticle porosity is variable.

Porous media characterisation

Pore structure was described in terms of porosity, pore size distribution (quantified by the mean pore size, r_M,) and specific surface area, SSA, whilst characterisation was carried out using mercury intrusion porosimetry, the nitrogen absorption technique and the helium pyknometer.

Mercury porosimetry is extensively used for the characterisation of porous media. The connected porosity, ϕ_{Hg}, and mean pore size, r_M, were obtained by Autopore IV 9500 Micromeritics mercury porosimetry (Table 1). The pore size interval ranges from 0.003 to 200 μm.

The determination of the specific surface area, SSA, of the samples was accomplished by using the nitrogen absorption technique. The determination of the SSA was carried out through the BET method (Rouquerol et al. 1994) and the points in the relative pressure interval $P/P_0 = 0.1–0.3$ were analysed by using the ASAP 2010 Micromeritics apparatus (Table 1).

Table 1 Connected porosity, ϕ_{Hg}, and mean pore radius, r_M, obtained by mercury intrusion porosimetry, *SSA* Specific surface area, ρ_{bulk} bulk density, ρ_{grain} grain density, ϕ_T total porosity, *C* capillary absorption coefficient, *k* water permeability of the rocks

Sample	ϕ_{Hg} (%)	r_M (μm)	SSA (m^2/g)	ρ_{bulk} (g/cm^3)	ρ_{grain} (g/cm^3)	ϕ_T (%)	*C* [$kg/(m^2\ h^{0.5})$]	*k* (mD)
CQC-1	17.79	28.69	0.83	2.11	2.70	21.84	6.47	293.31
CQC-2	16.32	34.18	0.38	2.12	2.66	20.19	10.94	1251.33
CQS-1	14.31	0.08	10.22	2.26	2.70	16.25	0.86	0.004
CQS-2	15.65	0.33	9.85	2.17	2.72	20.05	1.25	0.226
CQS-3	18.83	1.48	8.42	2.11	2.72	22.26	2.48	13.98
CQS-4	14.18	0.15	12.25	2.26	2.71	16.80	1.23	0.011
CQS-5	21.79	0.46	4.48	2.06	2.70	23.66	3.26	10.59
CS	26.02	0.35	12.69	1.97	2.71	27.09	2.10	0.839
DS	19.52	6.71	0.69	2.22	2.80	20.46	8.40	228.00
QS	13.48	2.43	2.31	2.28	2.67	14.62	1.68	2.02

The dry bulk density, ρ_{bulk}, of a rock is defined as the ratio of its mass to its volume, including the volume of voids and grains. In the characterisation test, three dried samples were used in the form of 30 mm diameter × 60 mm height cylinders (Table 1).

The grain density, ρ_{grain}, of a material is defined as the ratio of its mass to solid volume and can be obtained by using the Helium pyknometer. The real density was obtained by means of an AccuPyc 1330 device. The total porosity, ϕ_T, was calculated using the following equation (Tiab and Donaldson 1996):

$$\phi_T\ (\%) = \left(1 - \frac{\rho_{bulk}}{\rho_{grain}}\right) \times 100. \quad (1)$$

Water transport characterisation

Water transport was characterized by means of liquid water permeability (saturated flow) and capillary imbibition (unsaturated flow). The capillary imbibition test is carried out using a continuous data recording. It allows automatic monitoring of the water uptake by the sample when its lower surface is in contact with the water reservoir. A schematic diagram of the experimental set-up is shown in Fig. 1. The quasi-isolated chamber consists of a gastight methecrylate rectangle ($40 \times 40 \times 60\ cm^3$) wherein stable moisture and temperature are achieved. An environmental sensor (HOBO® H8-Pro) is also placed in the chamber in order to control the stability of the environmental conditions. The balance device is linked to a computer which automatically records weight gain in the tested specimen at specified intervals (every 10 s in the current study) using the code CK®.

Three cylinder samples measuring 30 mm in diameter × 60 mm in height were used in each test. The sample was hung from the balance and the water container ($20 \times 30 \times 5\ cm^3$) was raised with an elevator until water covers ~1 mm of the sample height. This level may be considered constant during the test. For example, if the porosity of sample is 20%, then it is fully saturated in the capillary imbibition test with ~8.48 cm^3 of water. Consequently, the decrease in the water layer in the container used is 0.14 mm. The temperature and relative humidity were constant throughout the experiment at 20 ± 1°C and 98 ± 0.5%, respectively. The results were plotted as absorbed water per area of the sample throughout imbibition versus the square root of time. Through this kind of representation, the capillary imbibition kinetic shows two parts. The first part defines capillary absorption and the second part defines saturation. The slope of the curve during capillary absorption is the capillary absorption coefficient, *C* (Table 1).

The continuous absorption method permits an extremely accurate characterisation of samples with

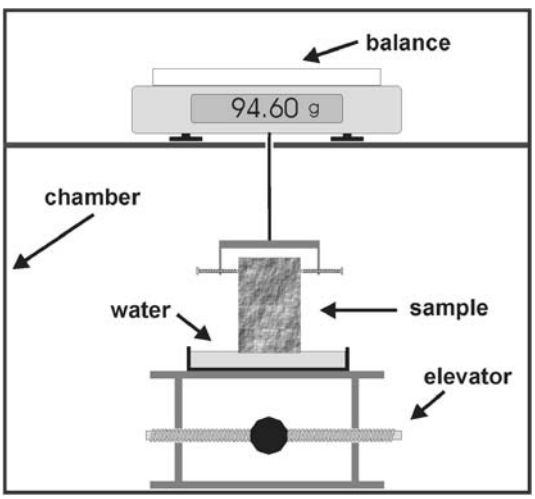

Fig. 1 Schematic diagram of experimental set-up for the continuous capillary imbibition characterisation

high absorption rates ($C > 10$ Kg/m^{2}h$^{0.5}$), in comparison with the non-continuous standard method. This is due to the fact that uninterrupted contact between the water and the sample is maintained.

The water permeability measurements were carried out in a triaxial cell (Fig. 2). Water permeability (intrinsic permeability) was determined according to Darcy's Eq. 2, when the steady-state flow was attained (water flow rate at inflow equals to water outflow rate):

$$k = \frac{\eta Q L}{A \Delta p}, \tag{2}$$

where k is the coefficient of water permeability (mD) ($1D = 9.869 \cdot 10^{-13}$ m^2), η the water viscosity, Q is the volumetric flow-rate of water, L is the length of the sample, A is the cross-sectional area of the sample perpendicular to the direction of flow and Δp is the pressure gradient (Bear 1988).

Pressure and volume changes were regulated by a pressure/volume controller, with accuracy below 1% in the pressure measurement and 0.5% over 100 cm^3 in the volume changes. The volumetric capacity is 250 cm^3. The volume changes and the confining and differential pressures are defined and controlled by using the Mecasoft code®, which displays the flow rate versus time on an X–Y plotter. A laminar (steady-state) flow rate with a constant pressure is achieved when the X–Y plot is a straight line. With this equipment, the permeability measurements are accurate for values below ~1D (~10^{-12} m^2 or ~10^{-5} m/s for pure water at 20°C). To reduce errors in the water permeability measurements, the confining pressure (2 MPa) was lower than the unconfined compressive strength, which ranged between 10 and 70 MPa for the studied samples (Table 1).

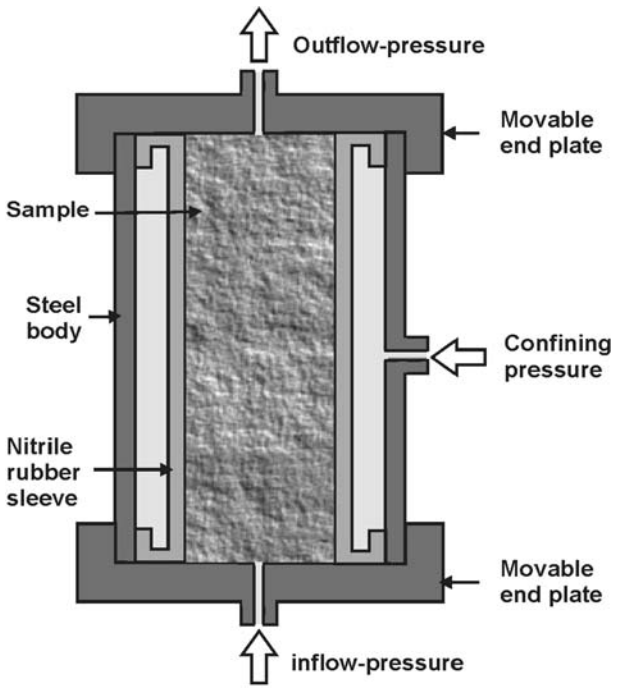

Fig. 2 Schematic diagram of triaxial cell for water permeability measurements

Permeability measurements were carried out using the same samples as those used in the dry density characterisation and in the capillary imbibition test. Thus, three cylinder samples measuring 30 mm in diameter × 60 mm in height were used after vacuum water saturation. The dried samples were placed in a vacuum at 20 ± 7 mbar pressure, in three 24-h cycles. The trapped gases in the porous system were eliminated during the first cycle. During the second cycle, samples were slowly introduced into distilled water over a 15 min period until they were submerged in 5 cm of water. They were then left there for 24 h. Atmospheric pressure was re-established and maintained throughout the last cycle.

Strength characterisation

Rock strength characterisation was performed by using uniaxial compressive and ultrasonic tests. The uniaxial compressive strength test is used to determine the maximum value of stress attained before failure. In the characterisation test, six samples were used in the form of 70 mm cubes and the load rate was 0.36 kN/s (Table 2). The samples were tested in accordance with the UNE-EN 1926 (Anon 1999).

The ultrasonic measurement was carried out with the same samples as those used in the water transport characterisation tests. The transmission method was used, which consists of two piezoelectric sensors coupled to the sample at constant pressure. One of the transducers is stimulated using an ultrasonic pulser and the other is used as a receptor sensor. Therefore, this method measures the propagation wave characteristics induced by microstructural factors. Compressional (v_P) and shear (v_S) wave velocities, dynamic elastic constants and waveform energy and attenuation were obtained from the digital analysis of the transmitted signal (Table 2).

Compressional (P) and shear (S) waves were measured using polarised Panametric transducers (500 KHz) and a Sonic Viewer-170, which acquired and digitalized the waveforms to be displayed, manipulated and stored. Visco-elastic couplants were used to achieve good coupling between the transducer and the sample. The P-wave signal was recorded using

Table 2 Compressional, v_P, and shear, v_S, wave velocities; dynamic Poisson ratio, v; dynamic Young's modulus, E; waveform energy, ϵ, attenuation α; uniaxial compressive strength, σ_C, and percentage of dry weight loss by salt crystallisation test, DWL, of the rocks

Sample	v_P (m/s)	v_S (m/s)	v	E (Gpa)	$\epsilon/10^{11}$	$\alpha/10^4(\mu s^{-1})$	σ_C (Mpa)	DWL (%)
CQC-1	5,075	2,843	0.27	43.31	1.11	2.05	19.9	1.0
CQC-2	4,976	2,824	0.26	42.70	21.49	5.49	20.9	1.5
CQS-1	4,029	2,477	0.20	33.24	50.33	5.42	35.5	13.8
CQS-2	4,080	2,614	0.15	34.18	43.19	4.95	27.9	3.2
CQS-3	3,920	2,377	0.21	28.87	27.38	7.14	23.5	7.2
CQS-4	4,008	2,472	0.19	32.93	23.68	5.20	34.3	8.1
CQS-5	3,462	2,121	0.20	22.21	2.50	2.94	13.7	16.3
CS	2,845	1,770	0.19	14.70	0.57	8.26	4.27	33.2
DS	4,017	2,546	0.16	33.58	17.49	4.42	33.5	0.5
QS	4,232	2,765	0.13	39.27	38.23	5.85	67.8	0.5

an ultrasound eco-gel, whereas the *S*-wave signal was enhanced by using a normal incidence couplant (SWC, shear wave couplant, GE Panametrics®).

The dynamic elastic constants of the rocks were calculated from the known ultrasonic wave velocities and bulk density, using the theory of elasticity (e.g. Christensen 1990; Guéguen and Palciauskas 1994; Tiab and Donaldson 1996). Thus, the Poisson ratio, v, and Young's modulus, E, were calculated as follows:

$$v = \frac{(v_P/v_S)^2 - 2}{2\left[(v_P/v_S)^2 - 1\right]}, \tag{3}$$

$$\mathrm{E} = \rho_{\mathrm{bulk}} v_P^2 \frac{(1-2v)(1+v)}{(1-v)}. \tag{4}$$

Waveform energy (ϵ) is presented in a dimensionless form and is defined as the integrate of the area under the square rectified amplitude:

$$\varepsilon = \int A_V^2 \mathrm{d}t. \tag{5}$$

The waveform attenuation (α) is obtained by fitting the positive part of the curve, A, to the first order decay exponential. In other words,

$$A = A_0 \mathrm{e}^{-\alpha t}, \tag{6}$$

where A_0 is the positive value of the highest waveform peak and t is the time. Due to the fact that the *P*-wave signal is more stable and reproducible than the *S*-wave signal, the energy and attenuation of signals is only obtained for the *P*-waves (Benavente et al. 2006).

Salt crystallisation test

The salt crystallisation test was performed using the continuous partial immersion test described by Benavente et al. (2001). Three samples were used in the form of $2.5 \times 2.5 \times 4$ cm prisms and a 14% w/w Na_2SO_4 solution was used. Resistance to salt crystallisation was found by performing the continuous partial immersion test, with 15 two-stage wetting–drying cycles, the stages being the capillary (40°C and 80% RH) and the precipitation stage (10°C and 70% RH). This is the procedure that most closely simulates the deterioration taking place in a construction material exposed to salt crystallisation. The samples were cleaned and dried (60°C) until they reached a constant weight. The dry weight loss (DWL) was calculated at this stage (Table 2).

Results and discussion

A principal component analysis (PCA) has been performed in order to establish the structure of the variable dependence. This involves identifying relationships between variables and in assigning a petrophysical meaning to each factor. The calculations were carried out using the SPSS® v.11.5.1 code. Two principal components (PC) were extracted which accounted for 86.5% of the total variance, using Varimax as a factor rotation method (Fig. 3). PC1 accounts for 45.1% of the total variation and is mostly linked to mechanical properties, porosity and density. PC2 accounts for 41.4% of the total variation and is associated with water transport and pore structure. Salt weathering, quantified by the percentage of weight loss after salt crystallisation, DWL, could be included in both principal components. This fact underlines the influence of mechanical properties, water transport and pore structure on the salt weathering of these porous building rocks.

The first component shows that there is a positive correlation between static and dynamic mechanical properties whereas a negative correlation with porosity is achieved. The relationship between uniaxial compressive strength, *P*-wave velocity and dynamic

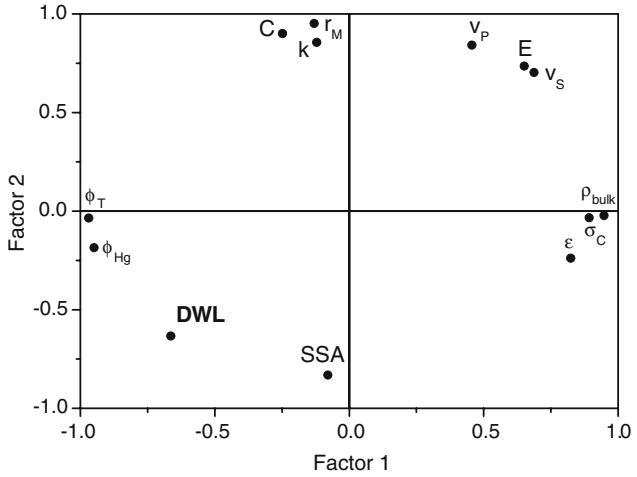

Fig. 3 Principal component analysis considering connected porosity, ϕ_{Hg}; mean pore radius, r_M; specific surface area, SSA; bulk density, ρ_{bulk}; total porosity ϕ_T; water absorption coefficient, C; water permeability, k; compressional, v_P, and shear, v_S, wave velocities; dynamic Young's modulus, E; waveform energy, ϵ; uniaxial compressive strength, σ_C and percentage of dry weight loss by salt crystallisation test, DWL, of the rocks

Young's modulus has been widely used in rocks, cements, concretes and bricks as ultrasound is a non-destructive method. However, *P*-wave velocity depends strongly on the elastic properties of rock-forming minerals. In particular, quartz is characterised by a relative low velocity (Schön 1996; Christensen 1990), and consequently, rocks with a high quartz content could result in a misleading characterisation (e.g. QS). The relationship between dynamic Young's modulus, *P*-wave velocity and bulk density can be explained using the theory of elasticity, as Eq. 5 shows.

A number of microstructural factors affect the reduction in waveform energy and wave velocity, such as boundaries between grains; the mineralogy, size and shape of grains and the presence of pore space and cracks. Thus, reflections, scattering, absorption and frictional dissipation of energy in these microstructural factors take place in different proportions to produce an overall attenuation of waveform energy. For example, rocks with high porosity values substantially reduce waveform energy. These microstructural factors influence the ultimate strength of the rock and control the direction in which failure occurs since they may act as surface weaknesses (Bell 2000). This explains the positive correlation between uniaxial compressive strength, *P*-wave velocity and waveform energy and attenuation obtained in the PC1.

The susceptibility of the porous rock to the salt crystallisation mechanism is closely connected to strength as it is the material's resistance to salt crystallisation pressure which creates tensile stress over the pore surface. This mechanical process can lead to disintegration, detachment and fracturation of the rock and, as a consequence, greatly decreases its durability (Scherer et al. 2001; Nicholson 2001). For this reason, rocks with high compressive strength, Young's modulus or ultrasonic wave propagation velocities tend to have a longer durability (Valdeón et al. 1996; Goudie 1999; Nicholson 2001; Benavente et al. 2004). This assertion explains the negative correlation of DWL and mechanical properties observed in the PCA.

The plot on the second component (PC2) shows that there is a positive correlation between water transport parameters (k and C) and mean pore radius, r_M, whereas a negative correlation with specific surface area, SSA, is registered. The relationship between permeability and pore structure can be described from the Carmen–Kozeny equation, which expresses permeability as a function of pore size, r, and porosity, ϕ, as follows (Bear 1988; Dullien 1992):

$$k = \frac{\phi r^2}{8}. \tag{7}$$

Moreover, this equation can be expressed in terms of surface area per unit of grain volume, S_{Vgr}, as follows:

$$k = \frac{1}{2S_{Vgr}^2}\left(\frac{\phi^3}{(1-\phi)^2}\right). \tag{8}$$

The specific surface area per unit of grain volume, S_{Vgr}, of a porous material is defined as the ratio of the surface area, A_S, exposed within the pore space to grain volume, V_{gr} (Dullien 1992; Tiab and Donaldson 1996). Hence, the specific surface area per unit of sample mass, SSA, is related to S_{Vgr} as follows:

$$S_{Vgr} = \frac{SSA}{\rho_{grain}}. \tag{9}$$

Consequently, permeability is inversely proportional to the square of SSA, $k \propto 1/SSA^2$, and reveals the inverse correlation between permeability and specific surface area obtained in the PCA.

The capillary flow is frequently interpreted by using the Washburn (1921) equation, which consists of applying the Hagen–Poiseuille equation to the movement of the liquid meniscus in the porous solid. If the gravitational term is negligible, the net pressure driving force is calculated as the difference between

the capillary pressures, Δp, which can be written by the Laplace's equation as

$$\Delta p = \frac{2\gamma \cos\theta}{r}, \tag{10}$$

where γ is the interfacial tension and θ is the contact angle. Therefore, the rise in the vertical direction, y, is described by the Washburn equation as

$$y(t) = \sqrt{\frac{r^2 \Delta p}{4\eta} t} = \sqrt{\frac{r\gamma \cos\theta}{2\eta} t} = B\sqrt{t}. \tag{11}$$

The capillary absorption coefficient, C, obtained in the capillary imbibition test, is closely related to pore structure by pore radius and porosity as follows (Mosquera et al. 2000; Benavente et al. 2002):

$$C = \phi\rho\sqrt{\frac{r\gamma \cos\theta}{2\eta}}, \tag{12}$$

where ϕ is the porosity and ρ is the water density. Equation (12) explains the association of C and r_M observed in the PCA.

Moreover, this statistical analysis indicates that there is a positive correlation between permeability, k, and capillary absorption coefficient, C. This association can be described inserting Eqs. (7) and (10) into (12) and then, the water absorption coefficient and permeability can be related as follows:

$$C = \phi\rho\sqrt{\frac{r\gamma \cos\theta}{2\eta}} = \rho\sqrt{\frac{2k\phi\Delta p}{\eta}}. \tag{13}$$

Thus, the capillary absorption coefficient is related to the square root of the permeability, $C \propto \sqrt{k}$, taking into account that the rock is comprised of parallel capillary tubes (Zimmerman and Bodvarsson 1991). A simple linear relationship between the square root of the permeability and capillary absorption coefficient is described for the studied rocks with $\phi > 10\%$ by:

$$\sqrt{k}\ (\mathrm{mD}) = -4.49 + 3.17C\ (\mathrm{kg/m^2 s^{0.5}}),\ R = 0.961. \tag{14}$$

Permeability measurements require more sophisticated equipment and experimental procedures than a capillary imbibition test. As a result, the permeability coefficient may be easily estimated for these kinds of porous materials from the capillary imbibition test, although further research into a wider range of rock types is needed in order to be able to fully apply the linear equation when estimating rock permeability.

The principal component analysis also shows the influence of water transport and pore structure parameters on the durability of porous building rocks under the effects of salt weathering. Damage from salt weathering, quantified by the percentage of weight loss after salt crystallisation, DWL, has a negative correlation with the mean pore radius and water transport parameters (k and C), and a positive correlation with specific surface area, SSA.

Salt damage is closely related to pore size. According to Everett (1961), crystallisation occurs initially in the larger pores forming large crystals from solutions supplied by the smaller pores. Scherer (2004) points out that maximum pressure occurs when a large crystal grows within a pore with small entries. It cannot penetrate to surrounding small pores until high saturation is achieved, producing great stress which damages materials (Steiger 2005).

Porous structure can be described simply as a bundle of pore throats and chambers, where the pore chamber is placed between the pore throats. Thus, the large pores account for most of the rock porosity, whilst the dimension and connectedness of the pore throats control the flow properties. One important topological parameter for the flow properties is the spatial average coordination number, z, which is defined as the average number of branches meeting at one node in the skeleton. Pore connectedness is related to a decrease in porosity of the coordination number of the pore space skeleton. With decreasing porosity, pore chambers and throats evolve differently, the throats shrink considerably and are eventually destroyed. Two porosity ranges can be distinguished with different porosity–transport property relationships in porous rocks (Wong et al. 1984; Bourbié and Zinszner 1985; Doyen 1988). Below 10% porosity, z dramatically decreases as a result of the closure and elimination of the throats, meanwhile in rocks where $\phi > 10\%$ the reduction of the transport coefficients with porosity is due almost entirely to the gradual reduction of the throat dimensions.

Consequently, it can be said that maximum crystallisation pressure occurs when a crystal grows in a pore chamber that is connected to a small pore throat. Thus, in rocks with large pore chambers that are linked to large pore throats (e.g. in CQC-1 and CQC-2), a large crystal grows in the pore chambers consuming high supersaturation and advancing through the pore space easily without creating any great pressure that might damage the rock. On the contrary, in rocks with small pore chambers linked to small pore throats (such as, for example in BC, CQS-1 and CQS-4) a small crystal

cannot penetrate to surrounding pore throats until high saturation is achieved, producing great crystallisation pressure which in turn causes damage.

Therefore, porous rocks ($\phi > 10\%$) with small pores and low water transport coefficient values (C and k) indicate a high susceptibility to salt weathering decay. However, this influence of pore structure and water transfer on durability may greatly vary depending on the nature of the building rock. Thus, porous materials with low porosity values have low water transfer coefficients (Eqs. 7 and 12), and are also more durable than highly porous rocks. For example, cemented oolite and microcrystalline limestones, granites or marbles present low porosity and permeability, and have excellent durability properties (Winkler 1997). Furthermore, the presence of cracks and fractures in building rocks leads to lower levels of rock durability (Nicholson 2001) and controls the water transport. However, their contribution to porosity may be considered to be negligible (Dullien 1992).

The specific surface area (SSA) of the materials is directly related to porosity and inversely related to pore size (Gregg and Sing 1982). Materials with high porosity but small pore size (e.g. CQS-1) presented a higher SSA than materials with a large pore radius and smaller porosity (e.g. CQC-1). From the PCA, the SSA appears to be directly related to damage from salt weathering (DWL values). Thus, high SSA values mean that a greater surface area of the material will be decayed. It is also inversely related to pore size and, therefore, directly related to salt crystallisation. Moreover, SSA plays an important role in the condensation process in porous materials since it is inversely related to pore size and, particularly, is intensely produced in pores with a radius lower than 0.1 μm when the Kelvin effect dominates. Thus, material with high SSA values implies a high capacity and susceptibility to water condensation and retention within the materials. The presence of solutions favours not only salt weathering but also material dissolution, absorption of contamination gases, freeze-thaw action and biodeterioration. In certain cases, the presence of a film of water may decrease the free surface energy of the material, weakening it. In other cases, for example in materials which contain clay minerals, water may alter the structure of the material, causing swelling, stress and fractures (Jiménez González and Scherer 2004).

The results from the principal component analysis have clearly established the dependence of salt weathering of porous rocks on its strength, water transport and pore structure, and assigned a petrophysical meaning to each factor. This approach can also be achieved for the studied rocks by means of a stepwise multiple regression analysis. This tentative model has been designed to assess salt damage related to the most common petrophysical properties, rather than using a predictive model given that this study deals only with Na_2SO_4 crystallisation. Thus, the percentage of dry weight loss by salt crystallisation, DWL (%), was taken as a dependent variable, while the mean pore radius, r_M (μm), connected porosity, ϕ_{Hg} (%), capillary absorption coefficient, C (kg/m^{2}h$^{0.5}$) and uniaxial compressive strength, σ_C (MPa) were considered as independent variables. This regression procedure gave a high multiple correlation coefficient ($R = 0.950$) (Fig. 4). There is a predominant statistical weight of σ_C^{-1} (0.559) in the prediction of the salt weathering, with a minor contribution by C (–0.183), r_M^{-1} (0.396) and ϕ_{Hg} (0.378). Moreover, this statement corroborates the importance of including both pore structure and rock strength in the estimation of the durability of porous building rocks proposed by Benavente et al. (2004).

Conclusions

In this study, the influence of water transport properties, pore structure and rock strength on the salt weathering of porous building rocks is approached using a statistical analysis. The principal component analysis has clearly established the dependence of salt crystallisation in porous rocks on their petrophysical properties, which is of particular interest for

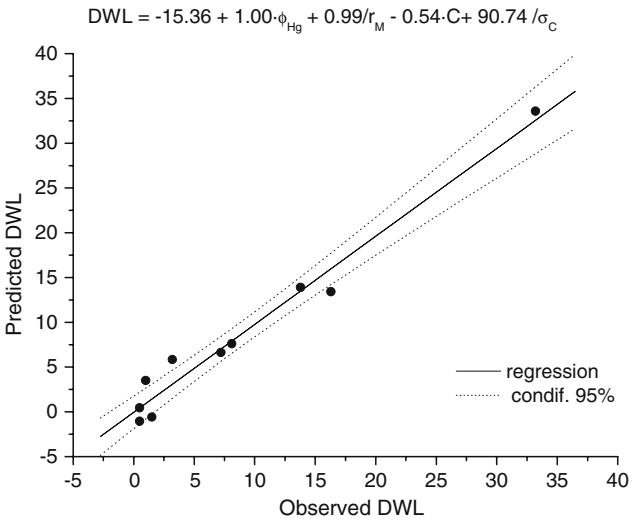

Fig. 4 Observed versus predicted values of percentage of dry weight loss by salt crystallisation, DWL, obtained by multiple regression analysis, considering mean pore radius, r_M, connected porosity, ϕ_{Hg}, capillary absorption coefficient, C and uniaxial compressive strength, σ_C, as independent variables

interpreting damage processes. Two principal components (PC) were obtained and assigned a petrophysical meaning. PC1 is mostly linked to mechanical properties, porosity and density, whereas PC2 is associated with the water transport and pore structure. Salt weathering, quantified by the percentage of weight loss after salt crystallisation, DWL, was included in both principal components, showing its dependence on their petrophysical properties.

Firstly, DWL has a negative correlation with uniaxial compressive strength, *P*-wave velocity, dynamic Young's modulus and waveform energy, whereas a positive correlation with porosity is achieved. This relationship can be established in terms of the microstructure which affects the reduction in waveform energy and wave velocity, and influences the material's resistance to salt crystallisation pressure.

Secondly, DWL has a negative correlation with the mean pore (throat) radius and water transport parameters (k and C) for the studied porous building rocks ($\phi > 10\%$). A practical relationship between the water absorption coefficient and the square root of the permeability has also been found. In porous rocks where $\phi > 10\%$, the reduction of the transport coefficients with porosity is due almost entirely to the gradual reduction of the throat size (Doyen 1988), whereas maximum crystallisation pressure occurs when a crystal growing within a pore chamber is connected to a small pore throat. Furthermore, a positive correlation between DWL and specific surface area, SSA, is also observed, which corroborates the inverse relationship of pore size with both SSA and salt crystallisation pressure.

Finally, a stepwise multiple regression analysis was carried out to assess salt damage related to the mean pore radius, connected porosity, capillary absorption coefficient, and uniaxial compressive strength, which are usually obtained in the petrophysical characterisation. This regression procedure shows that rock strength has a predominant statistical weight in the prediction of salt weathering, with a minor contribution of water transport and pore structure parameters.

Acknowledgments This study was financed by the Generalitat Valenciana (Spain) through the Research Project GV05/129 and Research Group 03/158.

References

Anon (1999) Métodos de ensayo para piedra natural. Determinación de la resistencia a la compresión. UNE-EN 1926

Bear J (1988) Dynamics of fluids in porous media. Elsevier, New York

Bell FG (2000) Engineering properties of soils and rocks. Blackwell, Oxford

Benavente D (2003) Modelización y estimación de la durabilidad de materiales pétreos porosos frente a la cristalización de sales. Biblioteca Virtual Miguel de Cervantes. http://www.cervantesvirtual.com/FichaObra.html?Ref=12011 (accessed on 15/06/2006)

Benavente D, García del Cura MA, Bernabéu A, Ordóñez S (2001) Quantification of salt weathering in porous stones using an experimental continuos partial immersion method. Eng Geol 59:313–325

Benavente D, Lock P, García del Cura MA, Ordóñez S (2002) Predicting the capillary imbibition of porous rocks from microstructure. Trans Porous Media 49:59–76

Benavente D, García del Cura MA, Fort R, Ordóñez S (2004) Durability estimation of porous building stones from pore structure and strength. Eng Geol 74:113–127

Benavente D, Martínez-Martínez J, Jáuregui P, Rodríguez MA, García del Cura MA (2006) Assessment of the strength of building rocks using signal processing procedures. Constr Build Mater 20:562–568

Bourbié T, Zinszner B (1985) Hydraulic and acoustic properties as a function of porosity in Fontainebleau sandstone. J Geophys Res 90:11524–11532

Christensen NI (1990) Seismic velocities. In: Carmichael RS (eds) Practical handbook of physical properties of rocks and minerals, CRC Press, Boca Raton pp 429–546

Doyen PM (1988) Permeability, conductivity, and pore geometry of sandstone. J Geophys Res 93:7729–7740

Dullien FAL (1992) Porous media fluid transport and pore structure. Academic Press, San Diego

Everett DH (1961) Thermodynamics of frost damage to porous solids. Trans Faraday Soc 57(9):1541

Goudie AS (1999) Experimental salt weathering of limestone in relation to rock properties. Earth Surf Process Landforms 24:715–724

Gregg SJ, Sing KSW (1982) Adsorption, surface area, and porosity, 2nd edn. Academic Press, London

Guéguen Y, Palciauskas V (1994) Introduction to the physics of rock. Princeton University Press, Princeton

Jiménez González I, Scherer GW (2004) Effect of swelling inhibitors on the swelling and stress relaxation of clay bearing stones. Environ Geol 46:364–377

Mosquera MJ, Rivas T, Prieto B, Silva B (2000) Capillary rise in granitic rocks: interpretation of kinetics on the basis of pore structure. J Colloid Interface Sci 222:41–45

Nicholson DT (2001) Pore properties as indicators of breakdown mechanisms in experimentally weathered limestones. Earth Surf Process Landforms 26:819–838

Rouquerol J, Avnir D, Fairbridge CW, Everett DH, Haynes JH, Pernicone N, Ramsay JDF, Sing KSW, Unger KK (1994) Recommendations for the characterization of porous solids. Pure Appl Chem 66:1739–1758

Scherer GW (2004) Stress from crystallisation of salt. Cement Concrete Res 34:1613–1624

Scherer GW, Flatt R, Wheeler G (2001) Materials science research for the conservation of sculpture and monuments. MRS Bull 26:44–50

Schön JH (1996) Physical properties of rocks: fundamentals and principles of petrophysics. Handbook of geophysical exploration. Section I, Seismic exploration, vol. 18. Pergamon, New York

Steiger M (2005) Crystal growth in porous materials—II: influence of crystal size on the crystallization pressure. J Cryst Growth 282:470–481

Tiab D, Donaldson EC (1996) Petrophysics: theory and practice of measuring reservoir rock and fluid transport properties. Gulf Publishing Company, Houston

Valdeón L, de Freitas MH, King MS (1996) Assessment of the quality of building stones using signal processing procedures. Q J Eng Geol 29:299–308

Washburn EW (1921) The dynamics of capillary flow. Phys Rev 17:273–283

Winkler EM (1997) Stone in architecture: properties, durability, 3rd edn. Springer, Berlin Heidelberg New York

Wong PZ, Koplik J, Tomanic JP (1984) Conductivity and permeability of rocks. Phys Rev B 30:6606–6614

Zimmerman RW, Bodvarsson G (1991) A simple approximate solution for horizontal infiltration in a Brooks–Corey medium. Trans Porous Media 6:195–205